

# AUV observations of mixing in the tidal outflow from a Scottish sea loch

T. Boyd, M. Inall, E. Dumont, C. Griffiths  
The Scottish Association for Marine Science  
Scottish Marine Institute  
Oban, Scotland, U.K.

**Abstract** - Freshwater outflows from estuarine systems carry nutrients, sediments, larvae and other materials into the coastal ocean where they mix into ambient ocean water. Loch Etive is one such estuary on the west coast of Scotland that is fed by a large rainfall catchment area, and from which the outflow is strongly modulated on a tidal basis. Freshwater leaves the loch on the ebbing tide in a pulse released into the coastal ocean as a thin layer, the leading edge of which develops into an undular bore or a train of internal solitary waves with strong mixing and associated entrainment.

A Hydroid 600 m depth-rated AUV equipped with a forward-mounted microstructure sensing package has been used in conjunction with moored measurements to study the dynamics of thin freshwater layers that are regularly released into the coastal ocean. During observations conducted in winter 2009 and spring 2010 we observed turbulent bores and internal solitary waves in Ardmucknish Bay, near the entrance to Loch Etive. The passage of the bores and internal solitary waves of depression were associated with downward vertical movement of near-surface water and turbulent mixing that was enhanced above background by over 2 orders of magnitude.

## I. INTRODUCTION

Improvements in observational capabilities have led to numerous observations of nonlinear internal waves (NIWs) over the past two decades and to increased attention to their role in redistributing energy and mass in the coastal ocean. Most of the observed NIWs have resulted from interaction of the barotropic tide with the continental slope or other bathymetric features and many of the resulting NIW packets were propagating shoreward over the continental shelf when observed [4,5]. More recently, it has become clear that rivers may act as sources of large amplitude internal waves in the coastal ocean [3,6]. Off the west coast of North America, the Columbia River plume is a tidally modulated source of fresh water onto the continental shelf, where the leading edge of the fresh water plume regularly evolves into a steep front from which packets of nonlinear internal waves emanate [3,6].

The sea lochs of the west coast of Scotland are estuarine systems that can be strongly modulated by the tide. Loch Etive is one such system with a relatively large catchment area, a fresh water outflow that is modulated semi-diurnally, and the outflow region of which has been known to exhibit

non-linear bore-like features following the tidal release of freshwater [1]. In this paper, we focus on observations in the outflow from Loch Etive under two considerably different sets of conditions: (1) in early winter following a prolonged period of precipitation during which the surface water is relatively cool (and temperature increases with depth) and brackish (i.e. salinity is low), and (2) in mid-spring following a relatively dry period during which the temperature decreases with depth and the surface salinity is relatively high.

Previous observations of the near-surface phenomena in the outflow from Loch Etive have focused on Ardmucknish Bay (Fig. 1), a small embayment north of the outflow region that is of order 1-2 km in length and width, with the major axis of the basin oriented just east of north, and which is of order 30-40 m depth in the center. The peninsula on the Northwest side of the bay, with steep bathymetry lying to the east, is a critical feature with respect to the evolution of these phenomena. Just east of the bay is a vantage point of 600 m elevation (Beinn Lora), visual observations from which have both motivated and guided these and earlier sampling efforts as well as interpretation of the observed phenomena.

## II. METHODS

The previous Ardmucknish Bay observations of Thorpe and Hall [1] describe the downstream evolution of the tidally pulsed outflow from Loch Etive as a positively buoyant gravity flow that spawns internal bore-like features and nonlinear internal wave (NIW) packets upon reflection from the steep bathymetry on the northwest side of the bay. The description of Thorpe and Hall, as well as frequent observations from Beinn Lora of surface banded structures associated with changes in reflectance due to compression and dilation of the capillary surface waves by NIWs led us to a sampling strategy that focused on repeated observations across the expected path of the reflected NIW field.

### A. AUV observations

The AUV observations discussed here were conducted with a Hydroid 600 m depth-rated REMUS vehicle, the front end of which was adapted to accommodate a Rockland Scientific International (RSI) mASTP turbulence microstructure

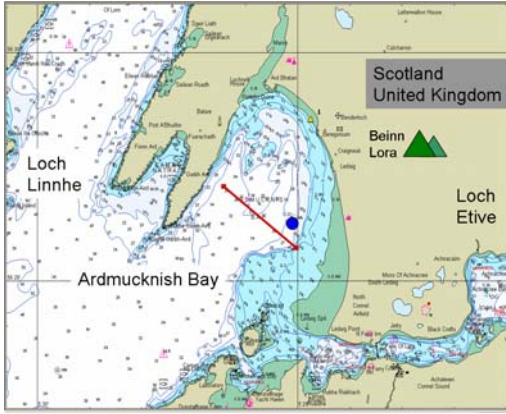


Figure 1. Map of Ardmucknish Bay showing the AUV transect location (red line) and mooring location (blue circle).

package [2]. The REMUS 600 AUV is a positively buoyant, propeller-driven vehicle that is 32.4 cm (12.75 in) in diameter and 2.74 m (108 in) in length, including the forward projecting guards that protect the microstructure sensors. The RSI mASTP includes two shear probes and two fast-response (FP07) thermistors, as well as a pressure sensor, and 3-D accelerometers which are used for evaluation of vehicle motion and in the computation of the Turbulent Kinetic Energy (TKE) dissipation rate ( $\epsilon$ ) [2]. The AUV was also equipped with a Neil Brown Ocean Sensors (NBOSI) conductivity-temperature (CT) sensor, and upward- and downward-looking RDI 600 kHz Acoustic Doppler Current Profilers (ADCPs), which are capable of measuring water velocity to a maximum range of 36-50 m from the vehicle, depending on bin size, and measuring vehicle velocity relative to the ocean bottom out to a range (i.e. vehicle altitude) of about 100 m. Subsurface navigation was accomplished by dead-reckoning between surface GPS fixes, assisted by bottom-track velocities, which were available throughout the missions described here, due to the shallow bathymetry throughout the study area.

Although turbulent mixing in the ocean is now most commonly studied using measurements obtained from free-falling vertical profilers, the earliest measurements of ocean turbulence were obtained from submersibles and towed bodies [13]. With the advent of robust autonomous vehicles, the oceanographic community has returned to horizontal measurements of turbulence, though this sampling mode is still far less common [2, 7, 14].

### B. AUV-based Microstructure Measurements

Sampling and data storage of microstructure data are carried out on-board with a separate science-payload PC104-based micro-processor running a linux operating system. Data acquisition begins automatically upon power-up of the AUV, with shear, FP07 and accelerometer channels at sampled at 512Hz. An analogue signal pre-emphasis, as described in

Mudge and Lueck [8], is applied prior to signal digitization. Data are written in binary format to a single file which is closed on power-down. In the present configuration no information is passed between the AUV hotel and the RSI payload. After the conclusion of sampling and recovery of the AUV, the RSI binary data file is transferred from the on-board PC104 via Ethernet for post-processing.

Microstructure shear probes output a DC voltage,  $V$ , which is proportional to the change in force applied to the tip of the probe in a direction perpendicular to the long axis of the AUV. For a probe moving at a speed  $U$  through the water, the horizontal (along-track) shear in a component water velocity ( $v$ ) perpendicular to the direction of travel is given by:

$$\frac{\partial v}{\partial x} = \frac{V}{2\sqrt{2GSU^2}} \quad (1)$$

in which  $G$  is the probe amplifier gain and  $S$  is the individual probe sensitivity. The shear signal is then high-pass filtered (at 0.5 Hz) to remove low frequency vehicle motion induced shear variance.

The dissipation rate of turbulent kinetic energy per unit mass (TKE) for isotropic turbulence can be calculated from the variance of the shear time series, according to:

$$\epsilon = 7.5\mu \overline{\left(\frac{\partial v}{\partial x}\right)^2} \quad (2)$$

in which  $\mu$  is the dynamic viscosity of seawater, and the overbar denotes a time average. The mean variance term is calculated as the integral of the power spectrum for a segment of the shear time series between two physical wavenumber limits that define the inertial sub-range for isotropic turbulence.

For the purposes of this experiment the time series of shear ( $S(t) = \partial v / \partial x$ ) is divided into sections of three seconds duration ( $N = 3 \times 512$  data points). Each section is cut into five half-overlapping segments, each of 512 data points in length. The segments are de-trended and multiplied by a cosine window prior to performing a 512-point FFT. The five FFTs are averaged to give a mean spectrum for each three-second data section, using the Matlab function "psd". A frequency dependent correction is then applied to the shear spectra to account for the reduction in response of the aerofoil shear probes at high wavenumbers (small spatial scale turbulent motions), following to Macoun and Lueck [9].

Experimental measurements in laboratories and from a tidal channel [10] have shown that a universal shape applies to the wavenumber spectrum of turbulent velocity fluctuations. The canonical spectral shape (shown as a dashed line in Figs 2a and 2b) is characterised by gradual rise from low wavenumbers, with a broad peak, followed by a higher wavenumber falloff at characteristic slope of  $k^{-5/3}$ , as predicted on dimensional grounds in Kolmogorov's original analysis. Viscous forces take hold around the Kolmogorov wavenumber (defined below), above which measured energy levels fall below the  $k^{-5/3}$  curve. As the energy of turbulent velocity fluctuations increases (and by implication also the rate of dissipation of TKE), the peak in the energy spectrum shifts to higher wavenumber, that is the length scale of most

energetic turbulent eddies decreases. The relationship between TKE dissipation rate  $\epsilon$  and shear variance (Eq. 2) suggests that the entire wavenumber spectrum of turbulent velocity fluctuations (i.e. all of the shear variance) must be resolved by measurements in order to accurately estimate the rate of TKE dissipation.

Shear spectra from the RSI package mounted on the REMUS AUV are found to have good overall agreement with the shape of the canonical Nasmyth spectrum between the wavenumber range of 0.5 to 55 cpm (Figs. 2a and 2b). At lower dissipation rates, however, the RSI spectrum (Fig. 2a) is contaminated with multiple narrow bandwidth spikes imposed on a broad shoulder of elevated spectral noise from 30 to 80 cpm. The wavenumbers of these spikes correspond to the fundamental and harmonics of the AUV propeller rotations and other broader bandwidth vibrational contamination, as determined by the ratio of noise-source frequency to vehicle speed. By applying the multivariate technique of Goodman [2], the vibrational contamination can be successfully removed by via cross spectral density estimates of the shear and vehicle acceleration channels, resulting in ‘cleaned’ spectra. The RSI measured spectral slope drops below the canonical  $k^{-5/3}$  above about 50 cpm, which is a feature not uncommon in shear microstructure measurements.

Finally, the cleaned spectra are integrated between appropriate wavenumber limits to give an estimate of the rate of TKE dissipation. The upper wavenumber limit is clearly defined by the Kolmogorov wavenumber  $k_K$  (indicated by the black arrow in Fig. 2b), the scale at which molecular viscous forces impede the turbulent motions:

$$k_K = \left(\frac{\epsilon}{\nu^3}\right)^{1/4},$$

in which  $\nu$  is the kinematic viscosity of seawater and  $\epsilon$  the dissipation rate of TKE. Should the TKE be sufficiently high that  $k_K$  exceeds the Nyquist limit, the latter is chosen as the upper integration limit for computation of the dissipation rate.

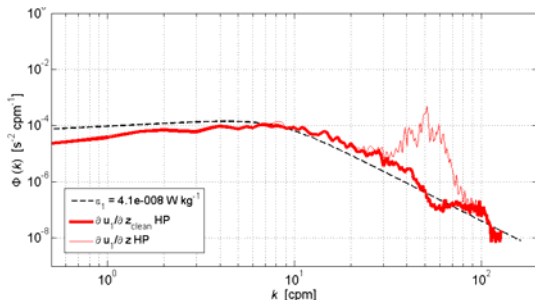


Figure 2a: Power Spectrum of velocity shear for a 30 second record from one RSI microstructure sensor. The measured frequency spectrum is converted to an equivalent wavenumber spectrum using average vehicle speed of 2  $\text{ms}^{-1}$  (= approx 4 kts). The raw spectrum (thin solid line) exhibits narrow band noise due to vehicle acceleration caused by the prop shaft and other vehicle activities. The heavy line represents the shear spectrum after removal of shear variance correlated with vehicle acceleration. The dashed line is the canonical Nasmyth spectrum.

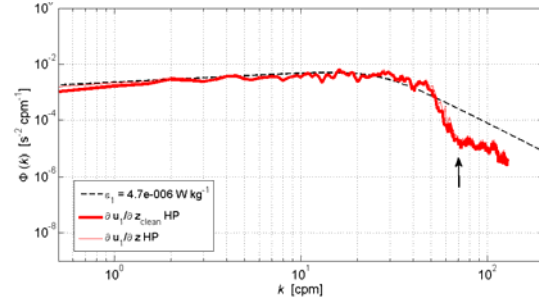


Figure 2b: As for Figure 2a for a 15 second record from one RSI microstructure sensor during a period of elevated turbulent activity. Kolmogorov wavenumber indicated by the black arrow.

The lower wavenumber integration limit is not as clearly defined, and is set empirically by consideration of the vehicle length. Assuming the vehicle responds significantly to fluctuations at greater than half the body length, this sets 0.75 cpm as a practical lower wavenumber limit, based on the REMUS 600 vehicle length of 2.7m.

The universal spectrum shown in each of the examples (Figs. 2a and 2b) corresponds to the dissipation rate calculated by integration of the measured spectrum over the limits described above. Preliminary analysis indicates that at measured dissipation rate estimates  $\epsilon$  below approximately  $2 \times 10^{-9} \text{ W kg}^{-1}$  the spectra become too contaminated with vehicle vibration to faithfully reproduce a  $k^{-5/3}$  shape (i.e. a -5/3 slope on log plot, as in Figs. 2) at high wavenumbers. At this stage it would therefore be prudent to state a noise level of approximately  $3 \times 10^{-9} \text{ W kg}^{-1}$  for the REMUS 600 TKE dissipation rate estimates.

### C. Auxiliary Measurements: CTD and Moorings

In order to place the AUV observations in the context of local tidal variability, we deployed an instrumented mooring in the bay for both of the AUV sampling periods described here. In each case, the mooring was instrumented with an upward-looking 600 kHz ADCP mounted on a gimbaled frame at the bottom, with two SeaBird Electronics (SBE) SBE-37 ‘‘microcat’’ conductivity, temperature, pressure sensors (one near-bottom and one near-surface), and several VEMCO temperature sensors. CTD casts were also conducted throughout the AUV sampling period in order to characterize the larger-scale spatial and temporal variability of the hydrographic fields.

## III. OBSERVATIONS

To simplify the data interpretation, most missions were run as a series of repeated transects over nominally reciprocal paths at a series of depths in the upper water column. These depths (5, 10, and less frequently 15 m) were chosen to be close to and just below the base of the surface layer

### A. December 2009 AUV Observations

Missions run on December 3, 2009 included two reciprocal path missions and a single-depth ‘‘lawnmower’’ mission. The

first mission consisted of reciprocal transects at 5m, 10m and 15m depth along the nominal path shown in Fig. 1, on headings of 125° and 305° (CW from North). The second mission consisted of a lawnmower pattern at 3 m depth with 4 rows parallel to and spanning the path of Fig. 1, and with row separation of 200 m. The final mission consisted of 3 reciprocal paths at 5 m and 10 m depths, parallel to but offset SW of the path of Fig 1.

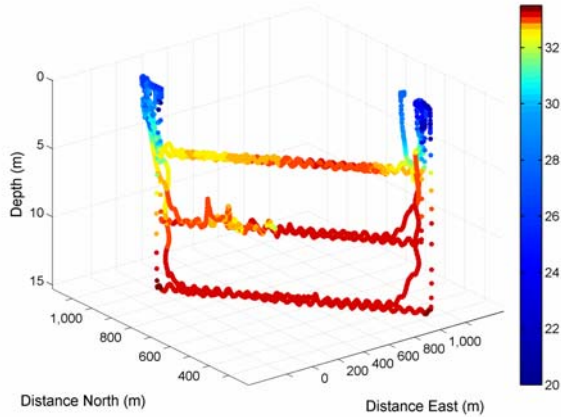


Figure 3. Along-track salinity from an AUV mission in Ardmucknish Bay on 3 Dec., 2009. The salinity stratification is largely confined to the upper 5 m. The lower salinity sections of the 10m transect result from downward movement of near-surface water associated with the propagation of a freshwater bore. The AUV track is shown as distance East of 5° 26.4'E and North of 56° 28.2'N.

This discussion is focused on the results from the first mission, consisting of six 1300 m-long segments. The AUV surfaced at either end of each of these segments and navigated by ADCP-assisted dead reckoning while submerged. The navigational accuracy was about 4% of the distance travelled underwater, resulting in up to 50 m errors at the surface waypoints over the approximately 1300 m path. The AUV speed was 3 kts (~1.5 m/s) throughout these missions, resulting in legs of approximately 14.5 minute durations, and a total mission time of 103 minutes, including the time for surface waypoints to obtain GPS position updates.

A composite of the salinity at the depth and position of the AUV throughout the first mission on Dec. 3 (Fig. 3) reveals that the greatest salinity (S) variability occurs in the upper 5 m, due to the presence of brackish (S=20-25 psu) surface water (see also Fig. 6) that has come out from Loch Etive when released by the ebbing tide.

The AUV-based ADCP measurements from this mission reveal that the near-surface water is moving northward over the entire path length in each of the six transects, but that the depth range of the northward current thins slightly over the course of the mission from the upper 3.5-4 m to 2-2.5 m, although the resolution of the very near surface is reduced during the later, greater transit depths due to sidelobe interaction with the surface at deeper bins. The overall similarity between the velocity structures in westward and subsequent eastward transects (Fig. 4) is a consistency check

of the AUV-based ADCP measurements, in the sense that there are no obvious direction-of-travel related velocity signatures. The most striking feature in the water velocity from this mission is the emergence in leg 3, subsequent eastward movement in legs 4 (Fig. 4) and 5, and eventual decay in leg 6 (not shown) of a strong front in the east (u) component of velocity in the upper 10 meters (Fig 3). The shallow region to the west of this front is also moving eastward in legs 3 and 4, though the region of eastward motion thins in legs 5 and 6. Note that there is also a deeper region (from 10 m depth to the bottom at 30-35 m) of westward flow beneath the eastward flowing bore and tail.

Estimates of the water velocity as the average over 4.5-8 m depth and over 50 second windows in the region immediately behind (west) of the leading edge of the front yield speeds of 12.3 cm/s and 14.9 cm/s in the directions 110° and 95° CW from North for the westward (leg 3) and eastward (leg 4) transects shown in Fig. 4, respectively. The standard deviation of the estimated average velocities is 0.80 cm/s, based on averaging over 7 ensembles each consisting of 4 water pings and 8 0.5 m bins, each of which have a single ping standard deviation of 12.86 cm/s in the absence of errors associated with vehicle motion. The temporal averaging interval of 50 s corresponds to a horizontal resolution of 75 m at an AUV speed of 3 kts (~1.5 m/s).

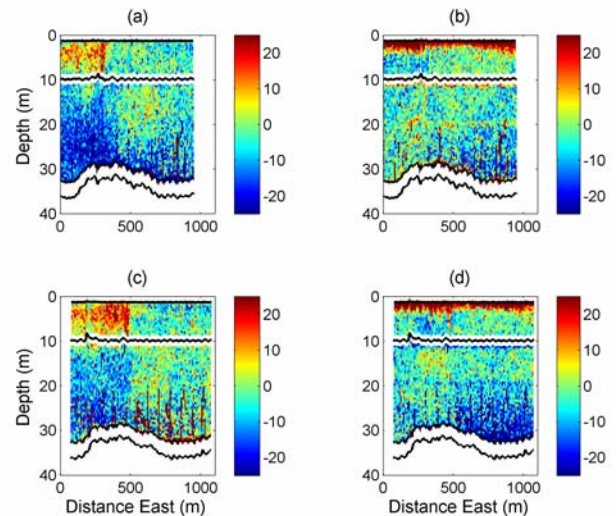


Figure 4. AUV-based ADCP-derived water velocity components above and below the AUV on repeated transects at 10 m depth on 3 Dec., 2009. Panels a (c) and b (d) show the eastward and northward components of velocity along the westward, leg 3 (eastward, leg 4) transect. The second (eastward) transect shows the eastward movement of the frontal location identified by the higher eastward velocities in panels a and c. Dark lines show the depth of the vehicle as well as the bottom depth and the depths of ADCP sidelobe contact with the surface and bottom.

While travelling at 10 m depth on legs 3 and 4, the AUV encountered an abrupt change in the temperature (T), salinity (S), and TKE dissipation rate  $\epsilon$  at the times/locations of the velocity front (Fig. 5). The temperature and salinity signals at these times are consistent with the downward displacement of

the mean T and S fields (Fig. 6) by approximately 5 m, as would be encountered at and in the wake of an internal bore or a packet of non-linear internal waves (NIWs) of depression riding on a thin near-surface density interface. The width of the front itself is quite narrow ( $\sim 6$  seconds or 9 m) as encountered by the AUV, and the width of the head of the bore-like feature is less than 50 m.

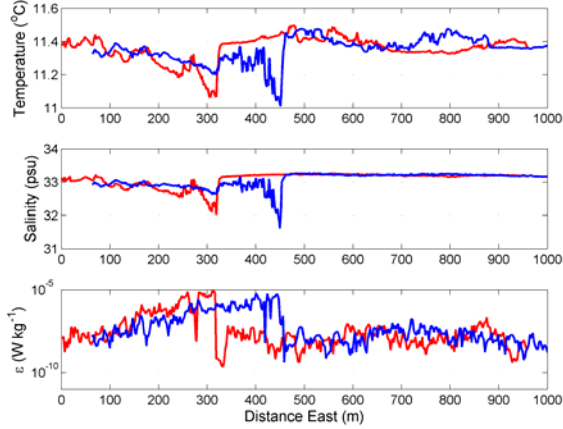


Figure 5. Time series of AUV-based measurements of temperature (top), salinity (center), and TKE dissipation rate (bottom) shown as distance East along the 10m transects from 5.44°W, showing the eastward displacement of the turbulent front, observed at 10 m depth, between the times of the westward, leg 3 (red) and eastward, leg 4 (blue) transects on 3 Dec., 2009.

Assuming that the water immediately behind (west) of the velocity front is moving in the same direction as the front itself, we have estimated the velocity of the front from the ADCP-derived water direction and the difference in encounter times and locations on subsequent legs. The bearing between subsequent encounters is  $118^\circ$  and derived speed projected onto the average direction of water motion ( $103^\circ$ ) is 23 cm/s. The heading between subsequent encounters (i.e. the net AUV direction of travel) is sufficiently close to the direction of water velocity that the error in the estimated average water speed exceeds the error that would have resulted from assuming the water motion was in the net direction of AUV travel. This velocity estimate is significantly less than the phase speed  $c = (gh\Delta\rho/\rho)^{0.5} = 35$  cm/s for an internal wave travelling on the interface beneath a 5 m thick layer with an average density anomaly of  $2.5 \text{ kg m}^{-3}$  as in Fig. 6.

The salinity and temperature signals in the wake (to the west) of the front in Fig. 5 do not return to the ambient, pre-front values, indicating that the rapid increase by over two orders of magnitude in values of  $\epsilon$  across that front result in mixing of the near-surface water, and are consistent with the observed sustained high levels of  $\epsilon$  in the wake of the front.

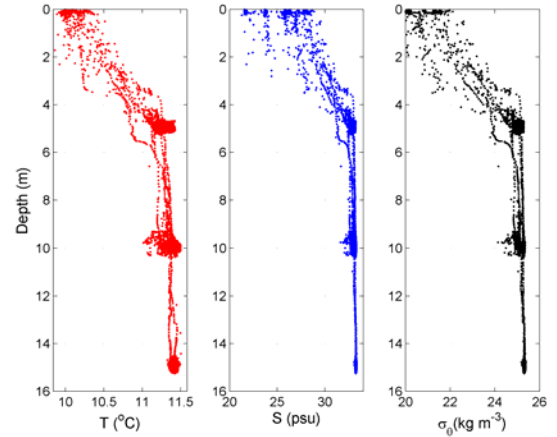


Figure 6. Temperature (T), salinity (S) and potential density ( $\sigma_0$ ) derived from the AUV during the mission shown in Fig. 3, for which ADCP velocity is shown in Fig. 4, and the 10 m T, S, and  $\epsilon$  are shown in Fig. 5.

### B. December 2009 Mooring Observations

Subject to the caveat that the mooring is close to the steeply sloping bathymetry at the eastern edge of the bay, the mooring data (Figs. 7 and 8) provide insight into the temporal variation of the temperature, salinity, and currents over the tidal cycle.

The mooring-based ADCP velocity measurements for the period of the December AUV observations (Fig. 8) reveal an intense northward and eastward near-surface current after day 337.4 similar to that observed throughout the transects, as shown in Figs. 4b and 4d.

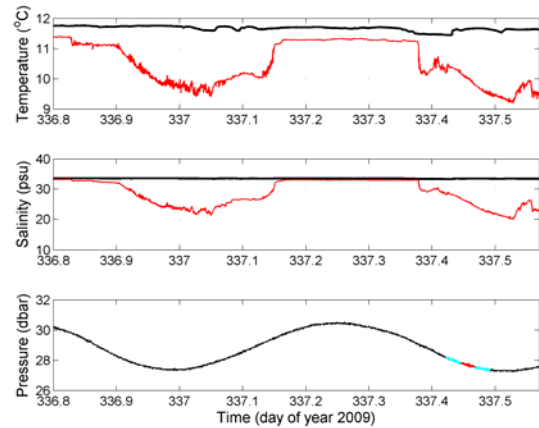


Figure 7. Time series of mooring-based measurements of near-surface (red) and near-bottom (black) temperature (top) and salinity (center), and bottom pressure (bottom), with the pressure during time frame of the AUV mission of Fig. 3 highlighted in cyan and the 10 m legs of that mission (Figs. 4 and 5) in red. Average depths of the instruments were 1.1 and 29.0 m over the 3 day deployment period.

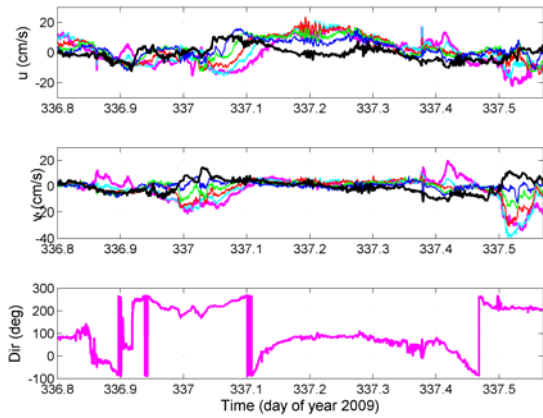


Figure 8. Time series of mooring-based measurements of the eastward and northward components of velocity at depths 4, 6, 8, 10, 12 and 18 m (magenta, cyan, red, green, blue and black lines, respectively) and the direction in CW degrees from North of the 4 m vector velocity. Velocity measurements were made with a bottom tripod-mounted 600kHz ADCP sampling 2m bins with 10.5 second ensembles of 50 pings, resulting in ensemble standard deviations of 0.5 cm/s.

The mooring measurements do not, however, reveal the strong eastward velocities associated with the eastward moving front shown in Figs. 4a and 4c, which later transects (leg 6, not shown) show dissipate before reaching the SE end of the transect, near the mooring location. The mooring data also reveal a transition toward the end of the record from low vertical shear to very high shear (up to 40 cm/s over 8 m) with southwestward currents in the near-surface layer and northeastward currents at depth, which is consistent with the AUV-based measurements of the final mission (Fig. 9).

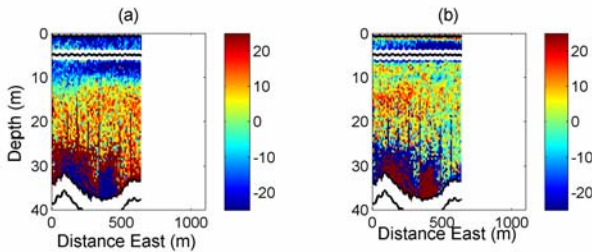


Figure 9. AUV-based ADCP-derived water velocity components above and below the AUV on repeated transects at 5 m depth on 3 Dec., 2009. Panels a and b show the eastward and northward components of velocity along an eastward transect.

### C. May 2010 AUV Observations

Analysis of the AUV data from December 2009 revealed that little additional insight into the evolution of the near-surface layer was gained from the single-depth “lawnmower” missions, due to the rapidly evolving nature and short spatial scales of the phenomena. For this reason, the missions conducted on May 19, 2010 consisted solely of repeated

transects at several depths over a single nominal path, in particular slightly off that shown in Fig. 1 (bearing 120° rather than 125°). The AUV observations of May 19 consisted of three missions, the first of which was 10 legs consisting of 1 “lap” (consisting of reciprocal transects) at 5 m, 3 laps at 10 m, and a final lap at 5 m. The second and third missions were conducted at 5 m and 10 m depth and consisted of 2 and 5 transects over the reciprocal pathway, respectively.

During the second mission, while the AUV was travelling westward at 5 m depth along the nominal path shown in Fig. 1, a westward and slightly northward flow is observed in the upper 7 m in the eastern half of the transect (Fig. 10). This corresponds to the positive temperature and negative salinity excursions seen at the same location (Fig. 11), which occur at the same time as a sharp increase in the TKE dissipation rate  $\epsilon$ . In this case, the downward displacement associated with the leading edge of the northward flowing gravity current results in a positive temperature excursion because the water temperature increases towards the surface as a consequence of seasonal warming.

By the time the northward moving front was encountered on the subsequent (eastward) leg, the single displacement peak has evolved into a rank ordered set of NIWs of depression, the leading waves of which have a length scales (at half-maximum) of order 15 m, though this estimate may be slightly compressed by the passage of the AUV against the presumed direction of propagation. Close consideration of the single depression of the first pass reveals a two tiered structure to the peaks in T and S, suggesting the beginning of the separation into a packet of waves.

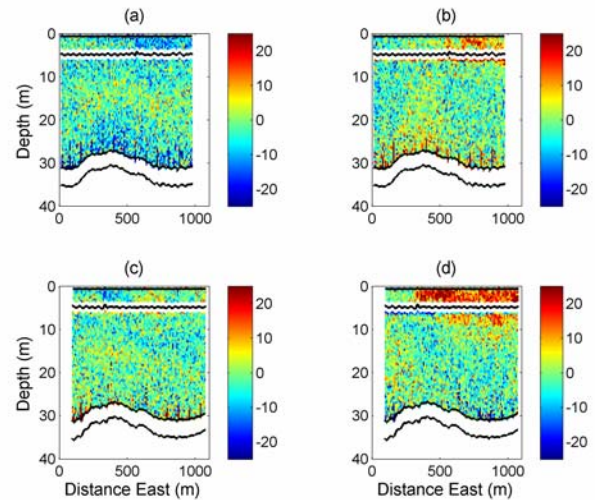


Figure 10. AUV-based ADCP-derived water velocity components above and below the AUV on repeated transects at 5 m depth on 19 May 2010. Panels a (c) and b (d) show the eastward and northward components of velocity along the westward (eastward) transect. The first (westward) transect shows a shallow northward and westward current East of 550 m. The second (eastward) transect shows the westward movement of the frontal location identified by the higher northward velocities in panels b and d.

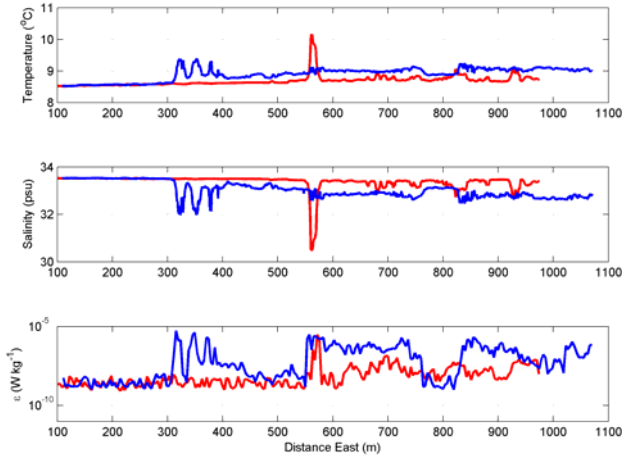


Figure 11. Time series of AUV-based measurements of temperature (top), salinity (center), and TKE dissipation rate (bottom) at 5 m depth shown as distance East along the transect from 5.44°W, showing the westward movement and evolution of a packet of the NIWs at the leading edge of the gravity flow between the first (westward, red) and second (eastward, blue) transects on 19 May, 2010.

In the record from the second (eastward) leg shown in Fig. 10, the TKE dissipation rate  $\epsilon$  is elevated both at the location of the NIW packet and in its wake, as well as at the location of and trailing the single peak from the previous leg (Fig. 11). This location of this increase in  $\epsilon$  corresponds to an increase in both temperature and salinity variance, as well as a shift in the magnitudes of T and S eastward of this location towards the surface values (higher T and lower S), suggesting that the fluid to the east of this location has been mixed, and because the  $\epsilon$  values are still high, is still actively stirring.

A lower estimate of the phase speed for the leading wave in the NIW packet can be obtained by assuming that it has emerged through amplitude dispersion from the single (possibly disintegrating) peak in the intervening period between the westward and eastward legs. The estimated speed based on translation of the leading edge of this feature is 33 cm/s on the bearing of 302°, just slightly off the nominal heading of 300° for this transect. In comparison, the water velocity measured by the AUV-based ADCP is 21 cm/s on a heading of 328° when averaged over the 1.6 to 3.1 m depth range and the 50 second period (approximately 75 m at 3 kts vehicle speed) following the leading edge of the first wave in the packet.

After the second encounter with the evolving NIW packet, there is a nearly 52 minute gap before the AUV next reaches the NW end of the transect. By this time, the shallow northward flowing layer has reached the NW end of the cruise track. After completing yet another lap the AUV encounters an eastward-propagating NIW packet near the NW terminus of the transect (Fig 13). This NIW packet was presumably generated by the interaction of a northward flow with the steep bathymetry on the west side of the bay (Fig. 1) [1].

Note that the apparent change in length scales (peak widths and separation) within the packet is due both to compression/dilation from the change in direction of AUV encounter as well as wave amplitude dispersion, and that the apparent wave dispersion is also affected by change in the AUV angle of encounter. The speed of the NIW packet is estimated from the translation between the AUV encounters on approach to and departure from the NW end of the transect as  $c = 18$  cm/s on a heading of 158°. This heading is significantly different from that of the nominal path, probably due to the accumulated navigation error at the end of the westward submerged path, but the heading error has little impact on the estimate of the speed. This estimated phase speed is significantly less than the linear phase speed ( $c=26$  cm/s) based on an average observed upper layer density anomaly of  $1 \text{ kg m}^{-3}$  for this period of the AUV sampling, and in which the upper itself was linearly stratified with  $N = 2.8 \times 10^{-2} \text{ s}^{-1} = 30 \text{ cph}$ .

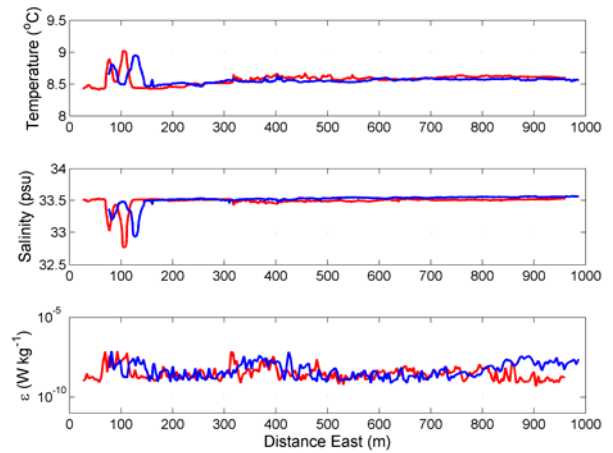


Figure 12. Time series of AUV-based measurements of temperature (top), salinity (center), and TKE dissipation rate (bottom) at 10 m depth shown as distance East along the transect from 5.44°W, showing the eastward movement and evolution of a packet of the NIWs after the gravity flow contacts the bathymetry at the west of the bay between the first (westward, red) and second (eastward, blue) transects on 19 May, 2010.

Unlike the earlier observation at 5 m depth of the westward propagating NIW packet, this packet observed at 10 m depth has neither an obvious signature in the velocity record (Fig 13) nor a significant increase in the TKE dissipation rate (Fig. 12).

#### IV. DISCUSSION

The processes by which fresh water as land-runoff mixes into the coastal ocean are of great interest to shelf sea modellers, to whom accurate representation of coastal salinity remains a significant challenge. Downward mixing of thin, fresh surface layers is an important feature to represent in models of the coastal ocean, yet measurement of near-surface turbulent fluxes (a pre-requisite to accurate model

representation) has been difficult to accomplish with conventional free-fall microstructure profilers, due to contamination of data within the upper 5 m by ship wake or profiler acceleration.

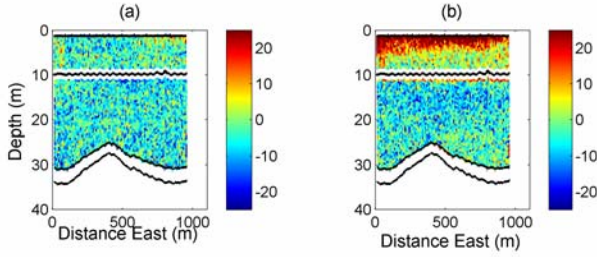


Figure 13. ADCP-derived water velocity components above and below the AUV on repeated transects at 10 m depth on 19 May 2010 sometime after the 5m transects of Fig 11. Panels a and b show the eastward and northward components of velocity along the westward (red) transect shown in Fig 12.

The present AUV-based measurements of the rapid and significant increase in TKE dissipation rate  $\epsilon$  by over two orders of magnitude from around  $10^{-8}$  to over  $10^{-6}$   $\text{W kg}^{-1}$  within and in the wake of the turbulent bores and non-linear wave packets are at high horizontal resolution and closer to the surface than most (though not all) such observations in the coastal ocean [12].

What causes the observed high levels of observed TKE dissipation rate? The linear density profile from the upper 5 m on December 3, 2009 (Fig. 6) corresponds to a very strongly stratified boundary layer with a Brunt-Vaisala frequency of  $N = (-g/\rho \partial\rho/\partial z)^{0.5} = 9.9 \times 10^{-2} \text{ s}^{-1}$  (=56 cph). Using  $N^2 = 3.05 \times 10^{-3} \text{ s}^{-2}$  as an upper estimate of the stratification together with the mooring-based measurements of shear between 4 m and 12 m depth (Fig. 8), yields  $Ri = N^2/u_z^2 = 1.2$  for the value of the Richardson number. This is well above the  $Ri=1/4$  Miles-Howard condition for instability, but sufficiently close (for  $N$  based on a mean profile) to suggest that shear instability across the base of the surface layer is a likely contributor to mixing. The shear levels observed at both the end of the moored time series (after day 337.5 in Fig. 8) and in the concurrent AUV velocity measurements (Fig. 9) are comparable in magnitude to the shear across the base of the reflected eastward moving turbulent bore (Fig. 4), suggesting that shear instability across that layer drives the elevated values of  $\epsilon$  in the wake of the bore.

What have these AUV observations contributed to our understanding of NIW and turbulent bore-like phenomena, and how can AUVs be effectively used to further our understanding? In the present case, the REMUS 600 AUV has provided:

- (1) water velocity measurements close to the air-sea interface (within 2 m of surface),
- (2) repeated observations of spatial and temporal evolution of features that are evolving rapidly in time and propagating in space (e.g. Fig 11),

- (3) observations close to the generation point of NIW packet, showing rapid evolution of a packet (Figs 11 and 12) and associated TKE dissipation, and
- (4) evidence of the mixed fluid in the wake of the bores and NIW packets (Fig 11), as well as
- (5) velocity and velocity shear measurements throughout the water column.

Although observed values of  $\epsilon \sim 10^{-5} \text{ W kg}^{-1}$  are not unusual for NIWs in the shelf seas, the presence of a turbulent wake in association with these features has been noted [5,11], but not adequately sampled. The use of an AUV as a measurement platform brings the potential for new insight into the horizontal extent of the influence of NIW's to the range of many wavelengths behind the wave or wave packet, and to reveal spatial relationships that would otherwise only be inferred through sequences of vertical profiles along the inferred pathway of these phenomena. The use of AUVs also introduces the potential for observation of the rapid evolution of high frequency processes, such as the amplitude dispersion of NIW packets.

Further insight into the mixing and dispersive effects of these phenomena can be gained through AUV-based mapping of an intentionally released dye such as rhodamine.

## V. SUMMARY

Several phenomena associated with the tidally pulsed release of a thin, relatively light surface layer from Loch Etive, Scotland, were observed with mooring- and AUV-based instrumentation during two periods of different hydrographic conditions.

In December, 2009, we observed the NW flow of thin surface layer, followed by SE propagation of bore-like feature with enhanced mixing both within the bore and in a long trail behind, with the implication that the bore has stirred up the near-surface fluid significantly.

In May 2010, two distinct phenomena were observed: (1) a single, sharp depression that dispersed into a later packet of NIWs propagating westward at the leading edge of a high dissipation region, and (2) an eastward propagating NIW packet after reflection of the gravity current at the west end of the bay.

As shown here, AUVs have significant potential to reveal aspects of near-surface and rapidly evolving small-scale phenomena with complex spatial structures, which would be otherwise difficult or impossible to observe and quantify. In this paper, we have focused on the near-surface phenomena associated with the release of fresh water from a sea loch, however it is evident from the AUV- and moored-velocity records shown here that these phenomena also have near-bottom, bathymetry-related expressions that would be amenable to study with the same AUV-based instrumentation we have used here.

## ACKNOWLEDGMENT

The work presented here is the result of testing and training opportunities conducted aboard the R/V *Calanus*, the master

and crew of which we thank for their good humour as we spun up to operating the AUV. Funding was partially provided by the UK Natural Environment Research Council and the European Regional Development Fund, under the Addressing Research Capacity (in the highlands and islands) project.

#### REFERENCES

- [1] S.A. Thorpe and A. J. Hall, "Bouncing internal bores of Ardmucknish Bay, Scotland," *Nature*, vol 306, pp.167-169, 1983.
- [2] L. Goodman., E. Levine, and R. Lueck, "On Measuring the Terms of the Turbulent Kinetic Energy Budget from an AUV," *J. Geophys. Res.*, 2006.
- [3] J. D. Nash, and J. N. Moum, "River plumes as a source of large-amplitude internal waves in the coastal ocean," *Nature*, vol 437, 400-403, 2005.
- [4] J. N. Moum, D. M. Farmer., W. D. Smyth, L. Armi, and S. Vagle, "Structure and Generation of Turbulence at Interfaces Strained by Internal Solitary Waves Propagating Shoreward over the Continental Shelf," *J. Phys. Oceanogr.*, vol 33, 2093-2012, 2003.
- [5] J. N. Moum, D. M. Farmer, E. L. Shroyer, W. D. Smyth, and L. Armi, "Dissipative Losses in Nonlinear Internal Waves Propagating across the Continental Shelf," *J. Phys. Oceanogr.*, vol 37, 1989-1995, 2007.
- [6] J. D. Nash, L. F. Kilcher, and J. N. Moum, "Structure and composition of a strongly stratified, tidally pulsed river plume," *J. Geophys. Res.*, vol 114, C00B12, doi:10.1029/2008JC005036, 2009.
- [7] S. A. Thorpe, T. R. Osborn, J. F. E. Jackson, A. J. Hall, and R. G. Lueck, "Measurements of Turbulence in the Upper-Ocean Mixing Layer Using Autosub," *J. Phys. Oceanogr.*, vol 33, pp 122-145, 2003.
- [8] T. D. Mudge and R.G. Lueck, "Digital Signal Processing to Enhance Oceanographic Observations", *J. Atmos. Oceanic Technol.*, vol 11, pp 825-836, 1994.
- [9] P. Macoun and R.G. Lueck, "Modeling the Spatial Response of the Airfoil Shear Probe Using Different Sized Probes.", *J. Atmos. Oceanic Technol.*, vol 21, pp 284-297, 2004.
- [10] P.W. Nasmyth, "Oceanic turbulence", *unpublished Ph.D. thesis, University of British Columbia, Vancouver*, 1970.
- [11] M.E. Inall, T. P. Rippeth and T. J. Sherwin. "Impact of nonlinear waves on the dissipation of internal tidal energy at a shelf break." *J. Geophys. Res* vol 105(C4): 8687-8705, 2000.
- [12] T. P. Stanton and L. A. Ostrovsky, "Observations of highly nonlinear internal solitons over the Continental Shelf," *Geophys. Res. Lett.*, vol 25, pp 2695-2698, 1998.
- [13] M. C. Gregg, "The Study of Mixing in the Ocean: A Brief History," *Oceanography*, vol 4, pp 39-45, 1991.
- [14] M. R. Dhanak and K. Holappa, "An Autonomous Ocean Turbulence Measurement Platform," *J. Atmos. Oceanic Technol.*, vol 16, pp 1506-1518, 1999.